Pulsed laser polishing of selective laser melted aluminium alloy parts

Debajyoti Bhaduri [a,b,*], Tina Ghara [c], Pavel Penchev [b], Soumitra Paul [c], Catalin I. Pruncu [b,d], Stefan Dimov [b], David Morgan [e]

[a] *School of Engineering, Cardiff University, Queen's Buildings, The Parade, Cardiff, CF24 3AA, UK*
[b] *Department of Mechanical Engineering, School of Engineering, University of Birmingham, Birmingham, B15 2TT, UK*
[c] *Department of Mechanical Engineering, Indian Institute of Technology Kharagpur, West Bengal, 721302, India*
[d] *Department of Mechanical Engineering, Imperial College London, South Kensington Campus, London, SW7 2AZ, UK*
[e] *School of Chemistry, Cardiff University, Main Building, Park Place, Cardiff, CF10 3AT, UK*

Abstract

Laser polishing (LP) of aluminium alloys by re-melting is particularly challenging due to their high thermal conductivity, diffusivity and reflectivity. In this research, a novel LP strategy is proposed to improve material's re-melting by introducing a thermally insulating ceramic baseplate during nanosecond-pulsed laser polishing of selective laser melted (SLM) AlSi10Mg parts in atmospheric and argon environments. The strategy considerably improves the material's re-melting as realised via sub-surface temperature measurements. This leads to a substantial reduction in the average roughness S_a (by ~80-88%) and neutral/compressive residual stresses (up to −19 MPa) when polishing in air with a laser energy density of 12 J/cm^2 and 10 scanning passes. In contrast, the unpolished SLM counterparts exhibit tensile stresses, up to +55 MPa. Laser polishing, however, somewhat reduces the Al parts' bulk hardnesses (by ~15-25%) compared to the as-built specimens. Heat affected zones (HAZ) in the form of Al-rich white layers up to a depth of ~35 µm beneath the LP surfaces are observed on the cross-sectional microstructures. The study reveals the importance of controlling the heat dissipation from the objects when laser polishing of thermally conductive materials to achieve the desired surface integrity properties.

Keywords

Laser polishing, aluminium, selective laser melting, surface roughness, residual stress, microhardness

1. Introduction

In today's Industry 4.0 scenario, digital manufacturing of parts is fostering greater uptake of additive manufacturing within the industry [1]. This has, in particular, promoted selective laser melting (SLM) of metallic materials for the production of near net shape complex geometries via a single processing step. Although SLM of aluminium alloys is particularly challenging due to the materials' poor flowability, high reflectivity and high thermal conductivity, a comprehensive study on the SLM of several aluminium alloys, in particular AlSi10Mg, has been conducted over the past decade and the process has been fairly optimised in terms of the finished parts' acceptable density, microstructure and mechanical properties [2]. This is mainly due to the AlSi10Mg alloy's good weldability, hardenability and corrosion resistance properties that lead to its numerous applications for the lightweight components in aerospace, automotive and electronic packaging sectors [2]. Despite these advantages, the SLM aluminium parts still suffer from high surface roughness (~4-15 μm) [3], balling, stair-step effects and adverse tensile residual stresses which could detriment the wear resistance and fatigue life of the components [4].

A viable route to improve the surface roughness/quality of the SLM parts is laser polishing (LP) which is clean, flexible, contactless and could be fully automated. The technology has been continuously developed over more than past two decades with early studies conducted on CVD diamond films, plates and fused silica specimens [5-7]. Much of the later LP research focussed on ferrous materials, predominantly involving tool steels [8,9], although several carbon [10] and stainless steel grades [11] have also been investigated. Similarly, the process

has been successfully employed for improving the surface morphologies of components made from nickel [12] and titanium [13] alloys.

Earlier research on LP of additive manufactured parts primarily centred on improving the surface finish of the as-built specimens. Remos-Grez and Bourell [14] investigated the use of non-tactile LP process for surface finishing of free-form selective laser sintered (SLS) iron-copper parts. Lamikiz et al. [15] reported an 80% reduction in surface roughness from 7.5 to ~1.2 μm R_a when operating at optimised LP process conditions on SLS AISI 420 stainless steel parts mixed with 40% infiltrated bronze powder. LP of SLM SS316L stainless steel cylindrical parts using a continuous wave CO_2 laser rendered a maximum reduction of the roughness R_a from 10.4 to 2.7 μm with no apparent significant change in the microstructure and microhardness of the material [16]. Another study on LP of laser clad SS316L specimens exhibited a substantial reduction in surface roughness of up to 96%, from 21 to 0.79 μm S_a [17]. Marimuthu et al. [18] developed a computational fluid dynamics (CFD) based numerical model to evaluate the melt pool dynamics during LP of SLM fabricated Ti-6Al-4V specimens. Experimental results involving optimised process parameters demonstrated an improvement in surface roughness from 10.2 to 2.4 μm. A comparable percentage reduction in roughness from over 5 μm of the AM Ti-6Al-4V parts to less than 1 μm after LP was also observed by Ma et al. [19]. Benefits of laser polishing further extended to an increase in surface hardness due to reduced porosity and dense microstructures within a depth of 100 μm, improved high cycle fatigue life by eliminating pores and reducing crack initiation and augmented cell biocompatibility [20]. Likewise, with regard to the AM nickel based superalloys, LP helped reducing average roughness R_a and 5-point average roughness R_z of SLM Inconel 718 samples from 7.5 μm and 31 μm to less than 0.1 μm and 0.6 μm, respectively [21]. A relatively lower percentage reduction (72%) in roughness was observed by Bures and Zetek [22] when employing LP on Inconel 718 surfaces produced via SLM, followed by machining.

Despite the reported benefits of laser polishing on steel, nickel and titanium alloys LP of aluminium alloys exhibits notable challenges, similar to those encountered during the SLM of Al alloys, due to the materials' high reflectivity, thermal diffusivity and large coefficient of thermal expansion [23]. Polishing by re-melting is aided by retention of heat input within the material. Thus, it is difficult to polish materials by laser re-melting that have high thermal conductivity and diffusivity. Aluminium alloys, such as AlSi10Mg has much higher thermal conductivity (~113 W/mK) in comparison to that of stainless steel 316L (~15 W/mK) and Ti-6Al-4V (~7 W/mK). Possibly because of this reason LP of the latter two materials have been more comprehensively studied [15-20]. In contrast, very limited research has been undertaken on the LP of Al alloys, where the materials were mainly forged and die cast [23, 24]. Research on the LP of SLM Al parts [25] is even more inadequate. Burzic et al. [23] investigated polishing of cast and subsequently ground AlSi9MnMg alloy using pulsed and continuous laser beams with varying laser intensity, feed rate and frequency. Reduction in surface roughness from R_a = 2.17-2.34 µm of the ground specimens to an R_a = 0.19 µm and R_a = 0.16 µm was achieved with the pulsed and continuous wave lasers, respectively. Similarly, improvement in surface finish was observed by Hofele et al. [25] following LP of SLM AlSi10Mg parts. The minimum R_a values recorded after single and multiple pass pulsed nanosecond LP were 0.66 µm and 0.14 µm, respectively, whereas R_a of the as-built SLM samples was in the range of 7.5 µm to 10.5 µm. Clearly, use of multiple laser passes rendered lower surface roughness.

The majority of literature on the LP of Al alloys has focussed on the evaluation of surface topography and roughness [23, 25-27], only a few papers has reported the effects of LP on the wear [24] and corrosion [28] resistance. Schmidt et al. [26] reported pulsed Nd-YAG laser polishing of forged AlCu4MgPb alloy and cast AlSi10Mg(Fe) alloy, with varying laser feed speed, hatch spacing and energy density (by changing the defocusing distance of the laser beam). The former material could not be polished due to surface crack formation. Conversely,

it was possible to polish the cast Al alloy that exhibited 66% reduction in R_a, from an initial roughness of 1.37 µm to 0.47 µm after LP. Furthermore, laser polished Al parts showed higher hardness and better wear resistance in comparison to the parent material, due to more uniform redistribution of smaller Si-rich phases within the laser processed areas [24]. Elahi et al. [27] observed development of an artificial oxide layer when LP of Al surfaces in atmospheric condition that led to an improvement in the wettability of the surfaces, thereby improved the weldability of the material when joined with a dissimilar material (polyamide in this case). Laser polishing was also reported to improve A2219 Al alloy's corrosion resistance without compromising the mechanical properties of the melted layer [28].

From the above literature review, it is realised that there is a huge scope to explore in depth the potential of LP for Al alloys. The present study investigates pulsed nanosecond laser polishing of selective laser melted AlSi10Mg aluminium alloy parts. The alloy is chosen for its widespread applications in the automotive and aerospace industry [29]. There is a recent trend to replace traditional cast components with additive manufactured parts within these sectors to reduce weight and energy consumptions during operation via topology optimisation. Laser polishing would be ideal for faster post-processing of these AM components at selective functional areas, compared to the conventional mechanical polishing such as vibratory finishing that would typically take 3-4 hours to reduce the roughness S_a from ~14-16 µm of the as-built SLM parts to ~4-8 µm after processing [30]. This research also explores the effects of introducing a thermally insulating baseplate under the SLM parts on the material's re-melting behaviour during LP. To the best of the authors' knowledge, such strategy during LP of Al alloys to aid re-melting has never been reported before. Additionally, in-depth analyses of wider surface integrity aspects such as residual stress, microhardness and microstructure of the aluminium parts polished under different environments (e.g. atmospheric, argon, nitrogen etc) are scarce in the published domain. As SLM process typically induce tensile residual stresses

within the built samples there is a scope to inspect the effects of LP as a post-processing step on the parts' residual stresses. Therefore, together with the surface roughness and topography evaluation this study undertakes a comprehensive evaluation of residual stress, microhardness and microstructure of the SLM AlSi10Mg specimens that are laser polished under atmospheric and argon environments.

2. Experimental details

2.1 Fabrication of selective laser melted Al Si10Mg parts

The SLM parts (10×10×7 mm^3) were produced using gas atomised AlSi10Mg alloy powders (nominal compositions given in [29]) supplied by LPW Technology Ltd., with a particle size range of ~20-63 µm, on a Concept Laser M2 Cusing® laser powder bed system, equipped with a Yb-fibre laser with 60 µm spot size and a vertical Z-increment of 30 µm. An island scanning strategy was adopted to balance the residual stresses in the specimens, details given in [29]. Parts were fabricated with a laser power of 250 W, beam scanning speed of 1500 mm/s, hatch spacing of 75 µm and island size of 2 mm, in an argon atmosphere with an oxygen-content <0.1%. Details of the SLM machine, powder material and processing conditions are given in Table 1. After selective melting the islands, laser scans were carried out around the perimeter of the layer with the same process parameters. For each subsequent layer, these islands were translated by 1 mm in the X and Y-directions as shown in Fig. 1.

Table 1. Details of the SLM machine, powder material and processing conditions

SLM machine	Concept Laser M2 Cusing® laser powder bed system
Powder material	AlSi10Mg alloy
SLM laser type	Yb-doped fibre laser
Laser beam spot size	60 µm
Vertical Z-increment/layer thickness	30 µm
SLM laser power	250 W
Laser beam scanning speed	1500 mm/s
Hatch spacing	75 µm
Island size	2 mm

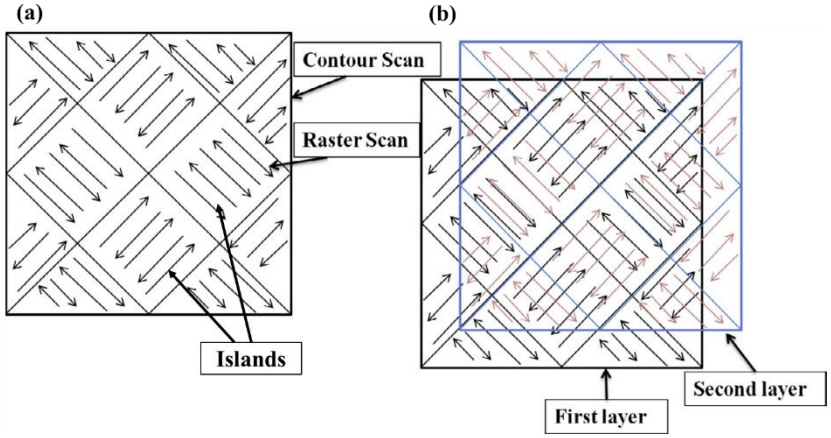

Figure 1. Schematic illustration of the island scan strategy, showing (a) each layer is divided into squares (islands) and the inside of the island is raster scanned, then (b) the successive layers are displaced 1 mm in the X and Y-directions [29].

2.2 Laser polishing of SLM Al Si10Mg parts

2.2.1 Phase 1 LP experiments

Laser polishing was carried out on the top face (upskin) of the SLM specimens (10×10 mm^2) on a Lasea LS5 laser micromachining system utilising a MOPA-based Yb-doped fibre nanosecond (ns) laser source with a maximum average power of 50 W, a beam focal spot size of 35 µm and a wavelength of 1064 nm. Following some preliminary trials to obtain the LP processing window, Phase 1 experiments were conducted in atmospheric environment using a full factorial design of experiments (DoE) comprising 9 tests with varying energy density, E_d (3, 6 and 12 J/cm^2) and number of laser scans (5, 15 and 25) over the 10×10 mm^2 area. The E_d

values were obtained using the equation $E_d=2(P/f)/(\pi d^2/4)$, assuming a Gaussian beam profile, when employing an average laser power (P) of 34 W, a defocussed beam of diameter (d) 85 µm and frequencies/pulse repetition rates (f) of 100, 200 and 400 kHz. Multiple laser scans were performed rather than the single scan strategy used in the authors' previous research on the LP of 3D printed (binder jetting) SS316L [31] and Ti-6Al-4V parts [32], because of AlSi10Mg's much higher thermal conductivity (~113 W/mK) compared to that of the latter two materials (~15 and 7 W/mK) [33]. The first laser scan direction covering the whole top surface (10×10 mm^2) was along the machine X+ direction. Each of the subsequent scan directions was aligned at an angle of 45° with respect to the previous direction, see Fig. 2. The laser pulse width, pulse distance and hatch spacing were kept constant at 220 ns, 2.85 µm and 3 µm, respectively, thereby achieving the pulses' overlaps along the beam scanning as well as in the transverse directions as ~97% in accordance with the optimised pulse overlaps in [31,32]. The variable and fixed LP process parameters in Phase 1 trials are shown in Table 2.

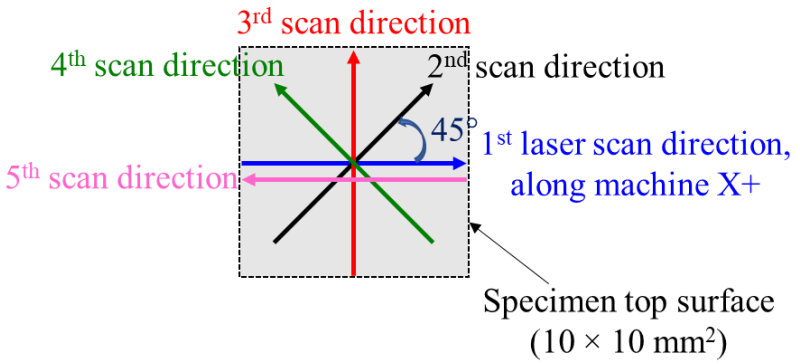

Figure 2. Schematic diagram showing the change in the laser scan directions, covering the whole 10×10 mm^2 top surface: The first scan direction is along the machine X+ axis while each subsequent scan is given anti-clockwise at an angle of 45° with the previous direction. The process is repeated for up to 25 scans.

Table 2. Variable and fixed LP process parameters in Phase 1 experiments

Variable process parameters			
Laser energy density, E_d (J/cm^2)	3	6	12
Number of laser scans	5	15	25
Fixed process parameters			
Average laser power (P)	34 W		
Defocussed beam diameter (d)	85 µm		
Pulse width	220 ns		
Pulse distance	2.85 µm		
Hatch spacing	3 µm		
Polishing environment	Atmospheric condition		

2.2.2 Phase 2 LP experiments

Based on the surface roughness results of the Phase 1 specimens and a few additional trials with a number of different scanning passes, 12 J/cm^2 laser energy density and 10 scans appear to give satisfactory surface roughness and quality within a reasonable processing time. Therefore, Phase 2 experiments were subsequently conducted using these laser operating conditions to investigate the effects of polishing environments, together with the introduction of a thermally insulating ceramic baseplate, on the material's re-melting behaviour. In particular, Phase 2 tests involved LP of six SLM samples in atmospheric and argon (Ar flow rate 11 L/min) environments (3 off samples in each condition) with 12 J/cm^2 E_d and 10 laser scans. An alumina ceramic baseplate (CB) was inserted under the specimens. It was anticipated that the thermally insulating ceramic baseplate (thermal diffusivity, α ~5.5-8.9×10^{-6} m^2/s) would reduce the heat dissipation from the AlSi10Mg samples (α ~4.7×10^{-5} m^2/s) through the Al 6082 workholding device (α ~7.1×10^{-5} m^2/s) [33].

Regardless of the energy density and the number of laser scans, hereinafter laser polishing in air without CB is referred as C1 condition and LP in air and argon with CB are denoted as C2 and C3 conditions, respectively, see Table 3.

Sub-surface temperature measurements during LP under C1, C2 and C3 conditions were conducted in three additional trials by placing two K-type thermocouples inside each specimen within a distance of 0.1 mm from the top face on which 15 LP scans (as shown in Fig. 2) were carried out at 12 J/cm^2 E_d. Temperatures were recorded by using an Omega® data logger at every 1 s interval.

Table 3. Notations for the laser polishing conditions

LP conditions	
C1	in air without ceramic baseplate
C2	in air with ceramic baseplate
C3	in argon with ceramic baseplate

2.3 Surface integrity analysis

2.3.1 Surface roughness, topography and composition analysis

At first, surface roughness and topography of the as-built SLM and laser polished specimens were carried out as reduction of roughness/improvement in surface quality is the prime objective of LP. The surface roughness was measured using an Alicona G5 InfiniteFocus microscope on a 2.7×2.7 mm^2 area at two locations, scanned with a 20× objective and the average was calculated. High resolution topography images were obtained via a Jeol JCM6000 scanning electron microscope (SEM), fitted with energy dispersive X-ray spectroscopy (EDS). Changes in the material's compositions following LP were detected using the EDS and X-ray photoelectron spectroscopy (XPS). XPS was performed on a Thermo Fisher Scientific K-alpha$^+$ spectrometer using a micro-focused monochromatic Al X-ray source (72 W) over an area of ~400 µm^2 at the centre of the polished surfaces. Data was recorded at pass energies of 150 eV for survey scans and 40 eV for high resolution scan with 1 eV and 0.1 eV step sizes respectively. Charge neutralisation of the sample was achieved using a combination of both low energy electrons and argon ions. Data analysis was performed in CasaXPS using a Shirley

type background and Scofield cross-sections, with an energy dependence of -0.6. Prior to this, to remove any loosely bound contaminating material, the samples were cluster etched by means of a Thermo Scientific MAGCIS source, operating in the cluster mode at 8 kV, with a cluster size of 1000 atoms and rastered over an area of ~2 mm^2. Sputtering was performed in a single 60 s interval.

2.3.2 Residual stress and phase analysis

In order to carry out extended surface integrity assessment of the LP parts the material's phase and residual stress analysis were carried out using a PANalytical Empyrean X-ray diffraction (XRD) instrument with Cu and Cr target, respectively. Phase identification was conducted within a 2θ range of 20° to 80°, at 45 kV voltage and 40 mA current, with a step size of 0.007°. Stress measurement was performed from 137° to 142.8° at 30 kV, 55 mA and 0.1° step size. Eleven stage tilt angles from -45° to 45° (0°, ±18.43°, ±26.57°, ±33.21°, ±39.23° and ±45°) were used for the stress measurement.

2.3.3 Microhardness and microstructure analysis

For the cross-sectional microhardness analysis, the specimens were sectioned via a slow-speed diamond saw cutter and the cross-sections were mounted and mechanically polished. Vickers microhardness measurements were carried out on the cross-sections, starting from the top laser polished face up to a depth of 200 µm, using a 5 g load and indent time of 15 s on a Leco LM700 microhardness tester. Two measurements were recorded on each sample, and the average was calculated.

Cross-sectional microstructures were revealed by immersion etching the specimens in Keller's reagent (2 mL hydrofluoric acid, 3 mL hydrochloric acid, 5 mL nitric acid and 190 mL deionised water) for 1 min 30 s and were observed under a Leica DMLM optical microscope.

The cross-sections were further characterised for changes in the grain size using a Hitachi 3400 SEM based Bruker e-flash electron backscatter diffraction (EBSD) detector operating at 20 kV acceleration voltage, 10 µA current density and 1 µm step size, with the images further post-processed using MTEX software.

3. Results and discussion

3.1 Evaluation of surface roughness and topography

The average area roughness (S_a) and 10-point area roughness (S_z) calculated from the roughness data recorded on two locations of the laser polished surfaces in Phase 1 experiments are shown in Figs. 3(a) and 3(b), respectively. The main effects of the LP parameters on mean S_a and S_z, obtained from the nine tests in Phase 1, are presented in Fig. 4. The main effect plots show that both surface parameters decreased with the increase in E_d from 3 to 12 J/cm^2 due to improved re-melting of the material at higher energy density. Similar observation was also made in the authors' previous study on LP of 3D printed SS316 parts where an energy density of 9 J/cm^2 provided better surface melting compared to that achieved at lower E_d of 5 and 7 J/cm^2. [31]. Higher standard deviations in the average and mean S_z values were generally noted for the processing conditions involving lower E_d (3 and 6 J/cm^2) and number of scans (5 and 15). This was due to the insufficient melting of material at these process parameters that caused greater surface irregularities. Conversely, S_a and S_z of the LP surfaces processed with 12 J/cm^2 E_d were lower by 46-70% and 79-83%, respectively, from that of the as-built SLM AlSi10Mg specimens (S_a: ~5.2-5.3 µm and S_z: ~183-232 µm). The minimum average roughness S_a obtained on the surface polished with 12 J/cm^2 E_d was 1.54 µm which was comparable or lower than the average roughnesses reported when LP of SLM steel or titanium, although in terms of R_a, that were approximately 1.5 and 2.4 µm, respectively [18, 34]. Mean S_z also decreased from

100 to 55 µm with the rise of the number of laser scans. However, increasing the number of scans extended the processing time. While the duration for 5 laser scans was ~10 mins, 15 and 25 scanning passes required ~30 and ~50 mins, respectively. Therefore, based on the surface roughness/topography results from Phase 1 and a few additional trials with 10 laser scans (20 mins of polishing time) it was decided to keep the energy density and number of scans constant at 12 J/cm^2 and 10, respectively, during the Phase 2 experiments in order to achieve an acceptable surface finish within a relatively shorter processing time. An alumina ceramic baseplate (CB) was introduced in Phase 2 to evaluate its influence on the material's re-melting behaviour. Furthermore, two different polishing environments, atmospheric and argon, were employed to assess their effects on surface melting as well as oxidation during LP. Apart from the six specimens produced in Phase 2 (3 off samples with 12 J/cm^2 E_d and 10 laser scans under air and argon environments, with CB underneath of them) three additional trials involving 12 J/cm^2 E_d and 15 laser scans were carried out under C1, C2 and C3 conditions to measure the sub-surface temperatures. The recorded temperature data, from the start of LP until cooling of the specimens to room temperature, are displayed in Fig. 5.

The surface parameters, S_a and S_z measured on the six LP specimens in Phase 2 experiments under C2 and C3 conditions are displayed in Fig. 6. It was observed that the thermally insulating alumina baseplate under the SLM specimens in Phase 2 tests considerably reduced S_a and S_z of the polished surfaces, with both parameters attaining values as low as 0.64 and 12 µm, respectively. Thus, a reduction by 80-88% and 92-95% from that of the parent SLM surfaces (~5.2-5.3 µm S_a and ~183-232 µm S_z) was achieved. This was evidently due to the improved re-melting of the material caused by the higher surface and sub-surface temperatures as observed via the temperature measurements. Maximum sub-surface temperature (~410 °C) in C2 condition was ~39% higher than that recorded in C1 situation (~295 °C), as seen from Fig. 5.

Regarding the surface topography, the as-built SLM surfaces exhibit balling formation, deep laser scan tracks and island boundaries on their top faces as shown in Figs. 7(a) and 8(a), obtained via the Alicona and SEM respectively. In contrast, the surface topographies of the LP parts subject to C2 environment, with 12 J/cm^2 E_d and 10 scanning passes display fine laser scan tracks, with no apparent pits or balling, see Fig. 7(b). An enlarged SEM image (Fig. 8(b)) shows the circular arc patterns formed on the LP surfaces due to material's re-melting and spreading under surface tension and gravity. However, despite the presence of the ceramic baseplate, further increase in laser scans (15 scans) aggravated the surface quality over a larger processing area, due to non-uniform melting, as evident from Fig. 7(c). LP in argon environment (C3 condition, with 12 J/cm^2 E_d and 10 scans) even further increased the S_a (~1.5-2.7 µm) and in some trials S_z (~45 µm in Test 6). A number of pits and key-holes are observed on the LP surfaces processed in argon, see images in Figs. 7(d) and 8(c). This was possibly due to the greater convective heat transfer from the parts' top faces caused by the flowing Ar gas, thereby deteriorating the material's re-melting. This is supported by the C3 temperature profile in Fig. 5 that shows ~24% lower maximum sub-surface temperature (~310 °C) compared to that recorded under C2 condition.

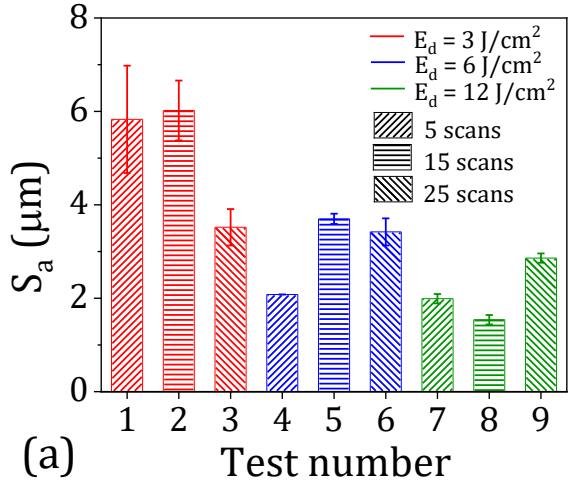

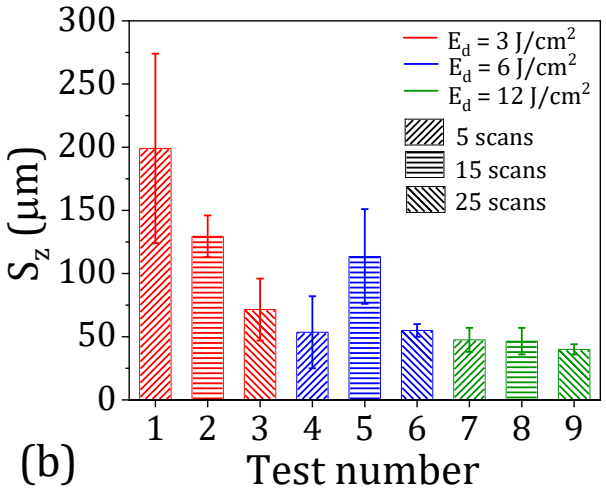

Figure 3. (a) Average S_a and (b) average S_z calculated from the recorded surface roughness data at two locations of the LP surfaces in Phase 1 experiments.

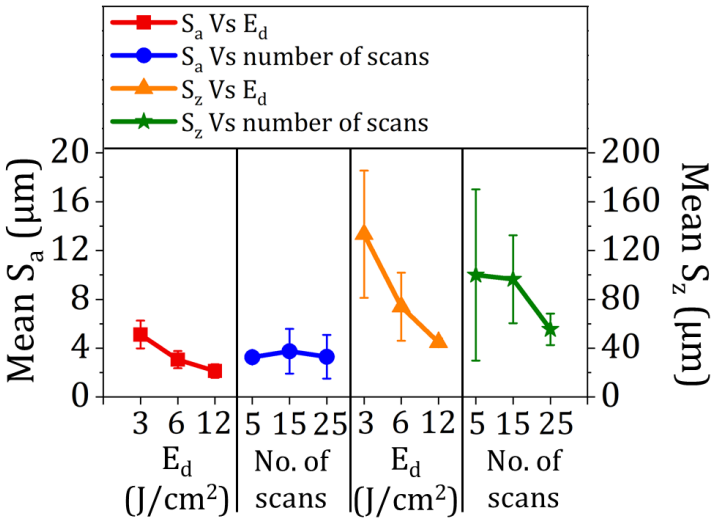

Figure 4. Main effects of the LP parameters on mean S_a and S_z in Phase 1 experiments.

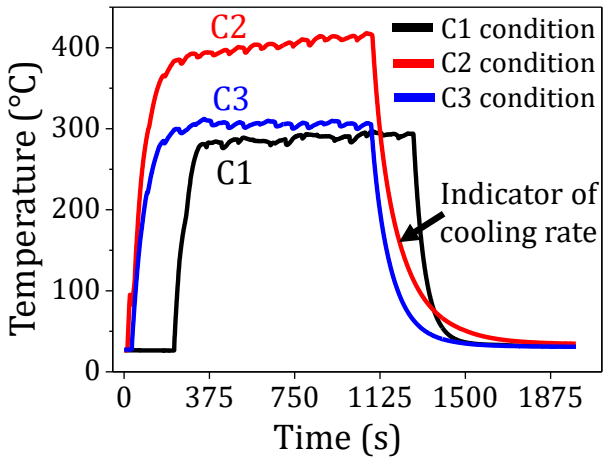

Figure 5. Sub-surface temperatures recorded during and after LP with 12 J/cm^2 E_d and 15 scanning passes.

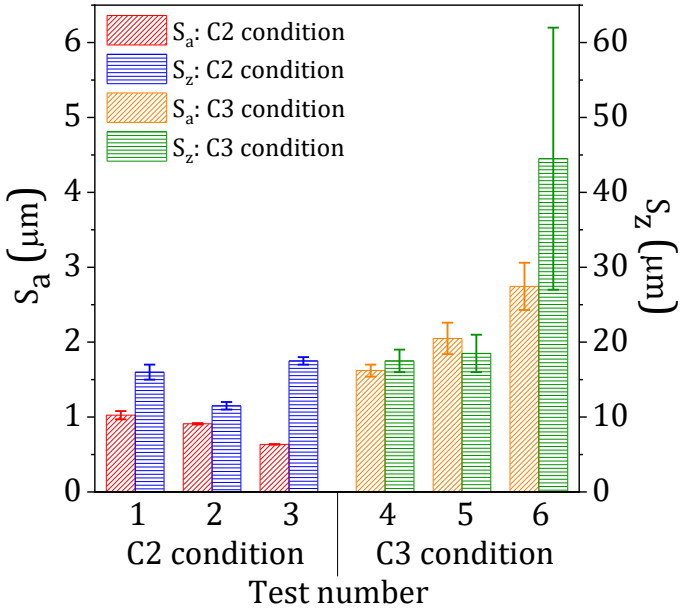

Figure 6. Average S_a and S_z calculated from the recorded surface roughness data at two locations of the LP surfaces in Phase 2 experiments under air and argon environments with the ceramic baseplate (C2 and C3 conditions, respectively).

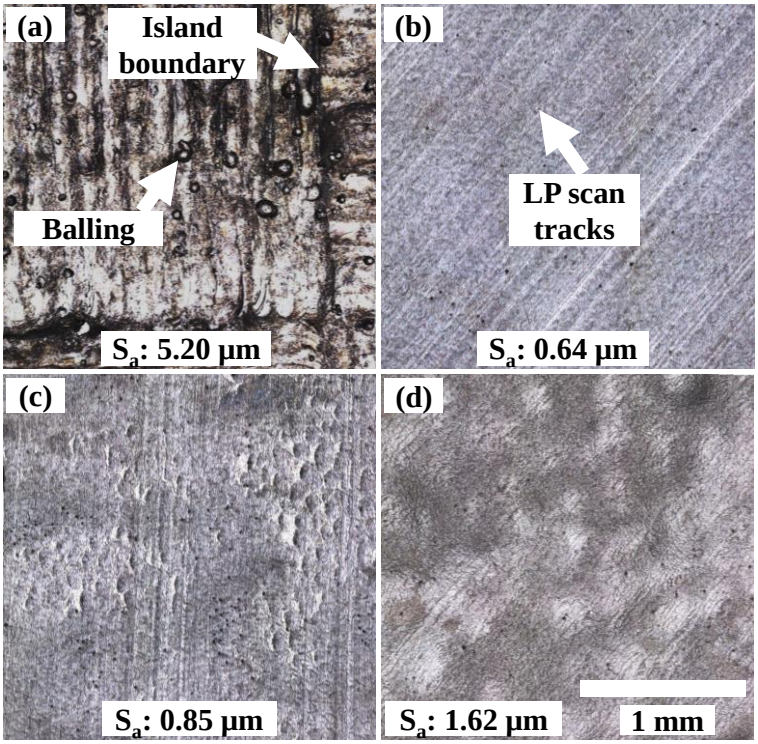

Figure 7. Surface topographies of (a) an as-built SLM part; and specimens laser polished with 12 J/cm^2 E_d and in (b) C2 condition with 10 scans; (c) C2 condition with 15 scans; and (d) C3 condition with 10 scans.

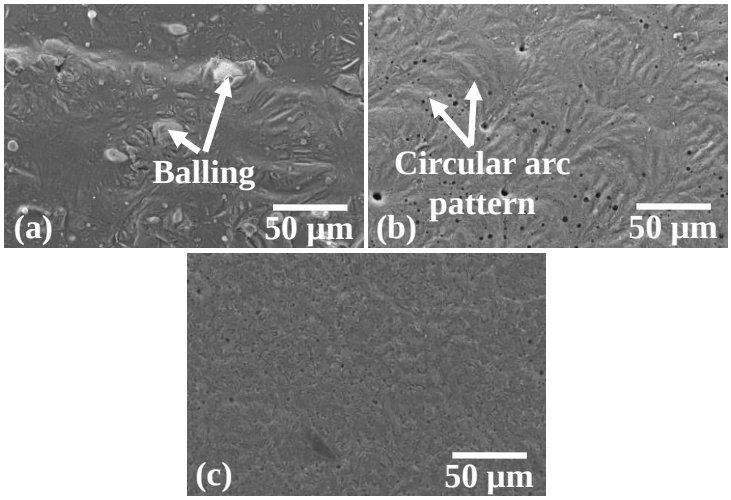

Figure 8. SEM of (a) an as-built SLM surface; and surfaces laser polished with 12 J/cm^2 E_d and in (b) C2 condition with 10 scans; and (c) C3 condition with 10 scans.

3.2 Analysis of residual stresses

In addition to its effects on the surface roughness/topography the use of CB and Ar environment further had clear influence on the residual stresses of the post-processed SLM parts, as observed from the measured stress data using XRD. Residual stresses measured on all the nine LP specimens from Phase 1 (equivalent to C1 condition) and six samples from Phase 2 (3 off under C2 and C3 conditions) are presented in Fig. 9. The Phase 1 LP samples without the CB and polished in air (C1 condition) exhibited tensile residual stresses, up to +106.1 ± 6.1 MPa when polished with 5 laser scans. The extent of tensile stresses typically reduced with the increase in the number of scans from 5 to 25, thought to be due to the increase in the part's surface as well as the bulk temperatures with greater number of scanning passes. This resulted in a reduction of the thermal gradient from the top LP face to the part's bottom face during the cooling period. The residual stress values further shifted towards more neutral or even compressive (−6.6 to −18.6 MPa) side when using the thermally insulating CB in Phase 2 that aided in reducing the

conductive heat transfer from the bulk body through the base/metallic workholding device. This is corroborated by the slower cooling rate observed in the C2 condition as shown in Fig. 5. Under the argon environment (C3 condition), convective heat transfer rate increased due to the heat extracted by the flowing Ar gas from the specimen surface, thus exhibiting relatively higher cooling rate during the cooling-off period compared to that in the C2 state, resulting in +3.1 to +27.1 MPa average tensile residual stresses. All as-built SLM samples showed average tensile stresses between +31.1 to +54.6 MPa.

The XRD phase analysis on the LP surfaces (Fig. 10) shows that the preferred Al grain growth direction gradually shifted from (111) plane to (220) plane with the increase in surface/sub-surface temperature as a result of either an increase in the number of laser scans from 5 to 25 (under C1 condition), or with the introduction of the ceramic plate (C2 condition). With higher convective heat transfer rate (i.e. higher heat dissipation rate) from the LP surface under C3 circumstance the preferred Al grain growth again shifted along (111 plane).

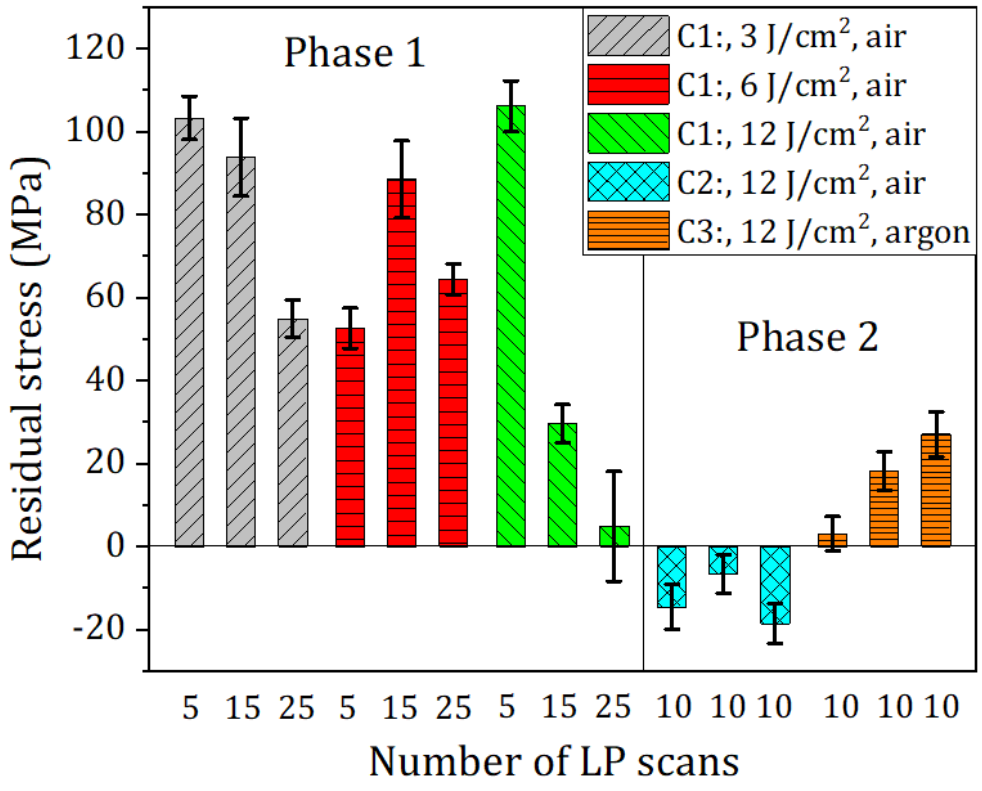

Figure 9. Measured residual stresses on the parts laser polished under air and argon environments with and without the ceramic baseplate

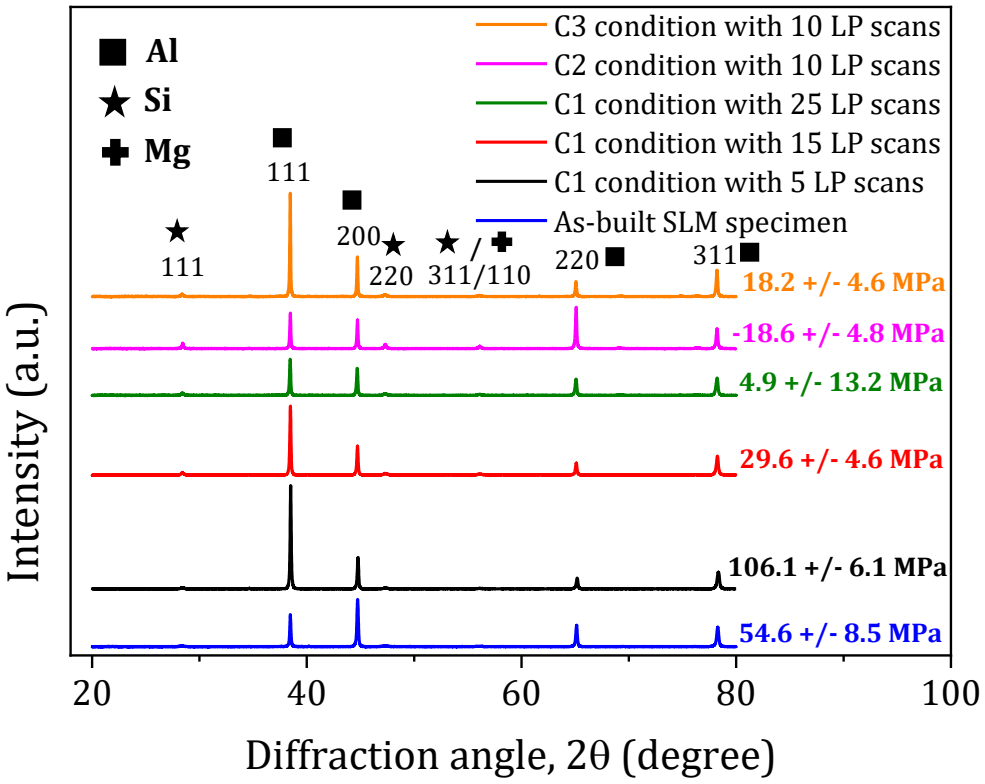

Figure 10. Representative XRD spectra and the corresponding residual stresses for as-built SLM and LP specimens processed with 12 J/cm^2 energy density under C1, C2 and C3 conditions.

3.3 Assessment of microhardness and microstructure

The effect of increasing the surface as well as bulk body temperatures during LP is assessed via microhardness depth profiles on the specimens' cross-sections. The microhardness depth profiles for LP specimens processed in air and argon, with and without the ceramic baseplate, are depicted in Fig. 11. While the as-built SLM samples exhibited roughly consistent hardness values of 95-108 $HV_{0.005}$ from a depth of 15 µm up to 200 µm (bulk hardness), the LP specimens displayed lower sub-surface and/or bulk hardnesses, depending on the surface and bulk body temperatures. Sub-surface layers with lower microhardnesses were observed on the LP parts under C1 condition, in particular when processed with 15 and 25 LP scans, with the softened region shifted farther from the top surface in the latter case (within 10-35 µm). This indicates that LP caused material's thermal softening and the thickness of the affected areas increased with the increase of number of laser scans. Sub-surface softened layers were also

observed on the LP specimens processed under C2 and C3 conditions, however to a lesser extent in the latter scenario. Indeed, the heat affected zones (HAZ) in the form of white layers are visible on the cross-sectional microstructures of C2 and C3 specimens in Fig. 12. By comparing Figs. 12(b) and 12(c) it is observed that the higher was the surface temperature (in C2 condition), the greater was the thickness of the LP affected layers (~30 µm in C2 with respect to ~22 µm in C3).

The overall rise in the parts' bulk temperatures as a result from the higher top surface temperatures under C2 and C3 conditions also caused reduction in the specimens' bulk hardnesses by ~15-25%. In contrast, the overall decrease in the material's bulk hardnesses was not so prominent for the parts polished under C1 conditions. Following the initial drop in the hardness values within the white layer zone (notably for the profiles obtained after LP with 15 and 25 scans) the microhardnesses increased again and became comparable with those of the as-built samples. As there was no ceramic baseplate under the specimens processed in C1 condition, the surface and bulk temperatures during LP were lower while the thermal gradient within the body during the cooling off period were higher with respect to the other two conditions. Therefore, the extent of thermal softening of the bulk body (beyond 35 µm depth) was not as great as compared to the samples polished with CB underneath them (purple and orange profiles corresponding to C2 and C3 conditions, respectively).

It is also worth mentioning that such overall softening of the material or formation of HAZ due to LP was not noted in the authors' previous study on the LP of 3D printed SS316L [31] and Ti-6Al-4V [32].

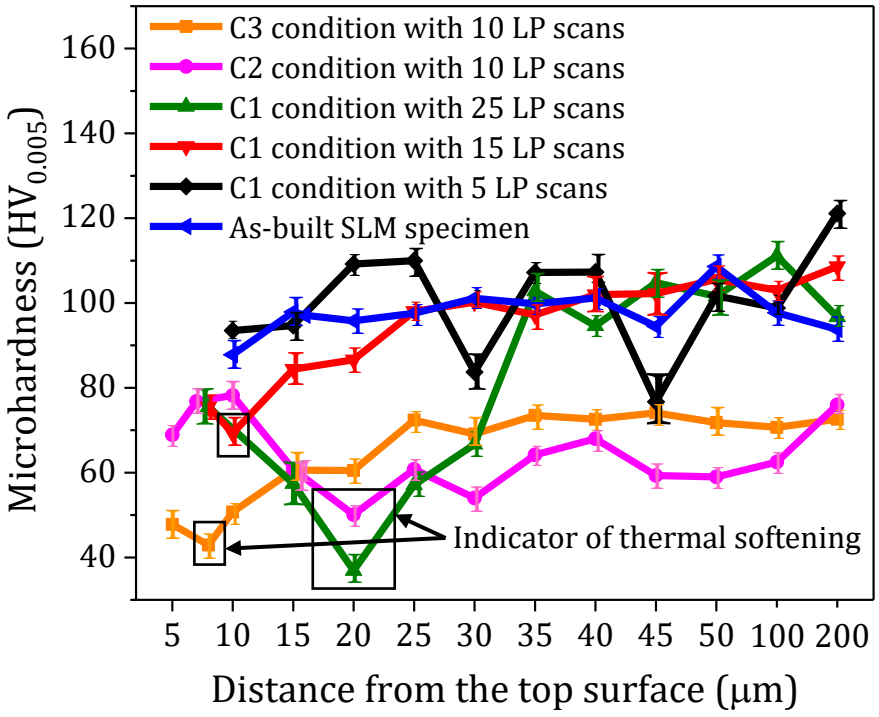

Figure 11. Microhardness depth profiles for as-built SLM and LP specimens processed with 12 J/cm^2 energy density and in air and argon environments with and without the ceramic baseplate.

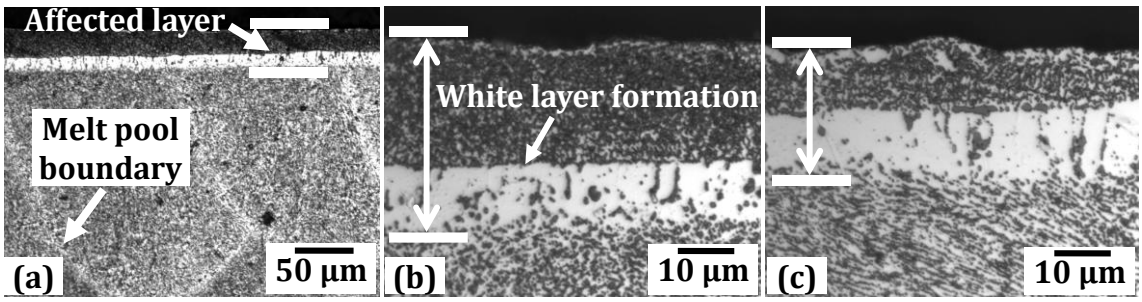

Figure 12. Cross-sectional microstructures of LP specimens processed under (a), (b) C2 and (c) C3 conditions.

The microhardness and microstructure results implied that possibly certain changes in the material's compositions due to LP had caused the sub-surface thermal softening/white layer formation. The compositions were analysed via EDS and XPS. The EDS area mapping on the cross-sections of the LP specimens (Fig. 13(a)) shows that there is a segregation between aluminium and silicon phases within the affected layers. The softer region, as noticed from the microhardness data, is rich with Al which has much lower bulk hardness than that of Si. The

LP surface also displays Si enrichment (~18-19 weight %) in Fig. 13(b) in contrast to the parent SLM surface where marginal presence of Si (~6 weight %) is observed (Fig. 13(c)). This observation is further validated by the XPS data in Fig. 14 that exhibits higher relative intensity of Si on the LP surfaces under both C2 and C3 (~19-20% atomic concentration) in comparison to the SLM surface (~14% at. conc. of Si). As Si has higher melting point (1414 °C) than that of Al (660 °C), the Al phases melted before the Si during LP. Chen et al. [24] also reported redistribution of Si-rich phases within the laser processed area. Furthermore, the incorporation of the insulating ceramic plate reduced the parts' cooling rates that led to the reduction of Si solubility in the liquid [35], thus increased the solute concentration. Hence was the segregation of Al and Si within the LP affected layers as detected by EDS and XPS.

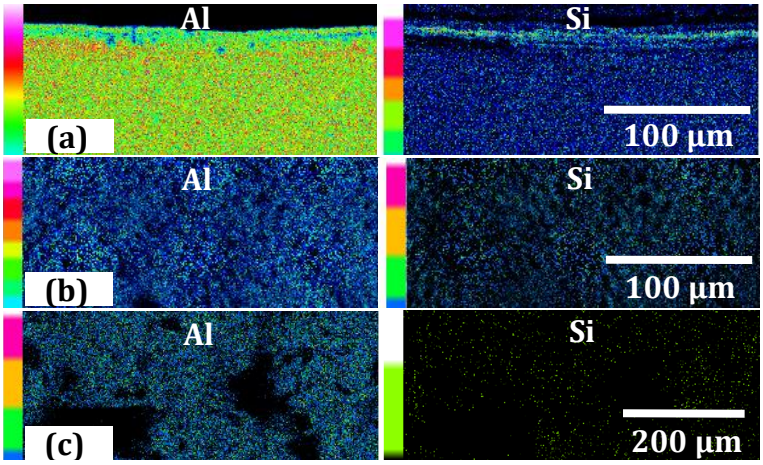

Figure 13. EDS area mapping on the (a) cross-section of the LP specimen and (b) LP surface processed with 12 J/cm^2 E_d and 10 scans under C2 condition; (c) as-built SLM surface.

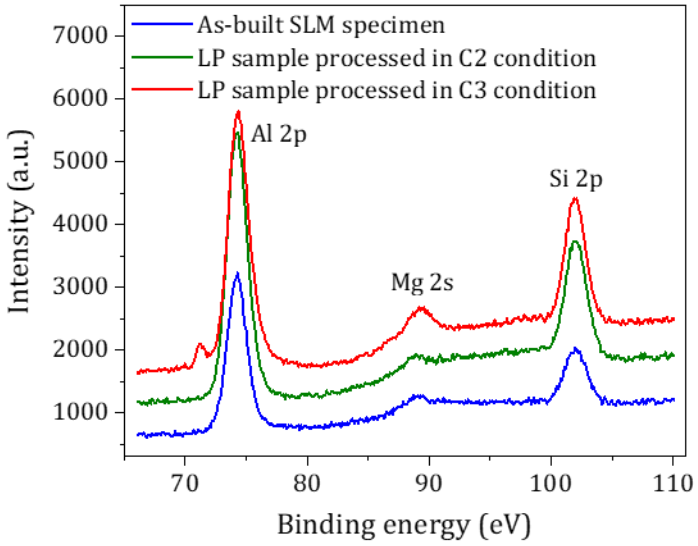

Figure 14. XPS spectra obtained for the as-built SLM and LP specimens processed with 12 J/cm^2 E_d and 10 scans in C2 and C3 conditions.

The changes in the sub-surface grain structures due to LP were revealed and compared with the parent SLM sample's grain structure via EBSD analysis. The EBSD inverse pole figures obtained on the SLM sample's cross-section display elongated grain growth along the built direction, with weak texture (Fig. 15(a)). The LP specimens show some signs of grain refinement up to a depth of ~25-30 µm. Fine, nearly spherical grains are observed beneath the LP surface processed under C2 condition (Fig. 15(b)). The grains abruptly became coarser below the fine grain zone which is probably the HAZ whereas the unaffected areas exhibit standard columnar SLM grain structures. The samples polished in argon do not particularly show any fine structures within the affected region, however irregular coarser grains are seen in the sub-surface, below which typical SLM grain structures are visible (Fig. 15(c)). Greater depth of the affected layers due to LP under C2 condition with respect to that processed under C3 environment is also noticed from Figs. 15(b) and 15(c). This is in agreement with the observations made from the microstructural analysis (Figs. 12(b) and 12(c)).

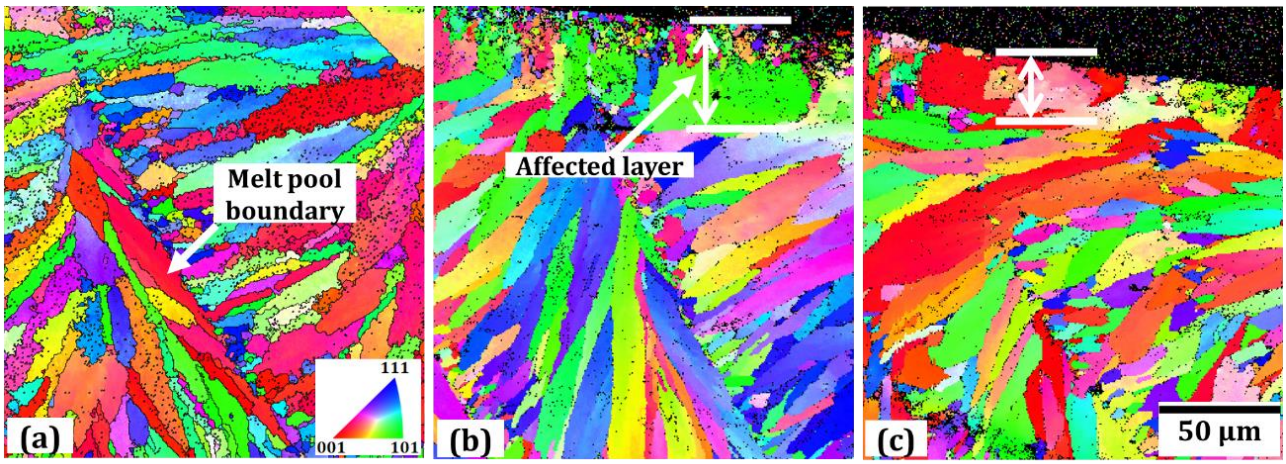

Figure 15. EBSD inverse pole figures taken on the cross-sections of (a) an SLM specimen, and on cross-sections of LP samples processed in (b) C2 and (c) C3 conditions.

4. Summary

The present research explores the potential of pulsed laser micro-polishing as a viable post-processing technique for additive manufactured (in particular, SLM) parts built from materials with high thermal conductivity and diffusivity. The effectiveness of LP in reducing the high surface roughness of SLM objects greatly depends on the materials' re-melting behaviour during polishing which in turn relies on their thermal properties. Thus, LP of highly thermally conductive materials, such as aluminium and copper alloys, is especially challenging. When processed with laser, the transition between the unaffected state to the ablation regime often abruptly takes place for these materials without undergoing through the melting regime. An example of this phenomenon was noted in a previous study by the authors during LP of 3D printed (by using binder jetting technique) copper alloy parts. The laser material interaction was dominated by mainly ablation, with only sporadic surface melting observed at certain regions [36]. Materials with lower melting points, such as aluminium (~660°C), even further aggravates the problem by narrowing the LP parameters' processing ranges. In order to circumvent these challenges, this study introduces a novel strategy to reduce the heat loss from

the AlSi10Mg parts during LP by introducing a thermally insulating ceramic baseplate under the specimens.

Following some preliminary trials and a full factorial design of experiments involving 9 tests, it is inferred that an energy density of 12 J/cm^2 and 10 laser scans would render an acceptable surface roughness and quality (minimum S_a measured ~1.54 µm). The quality of the polished surfaces even further enhances with the use of the insulating ceramic plate under the specimens. Through the experiments, it is evident that the insulating plate substantially increases the object's sub-surface temperatures (by up to ~39%) with respect to the temperatures recorded without the plate during polishing in atmospheric condition. The higher surface/sub-surface temperatures considerably improve material's re-melting which is supported by the specimens' lower surface roughness and smoother surface topographies. The minimum S_a obtained by using the ceramic plate during LP in air is ~0.64 µm, a reduction by ~80-88% from that of the parent SLM surfaces (~5.2-5.3 µm S_a). Thus, it is realised that a laser polishing route under atmospheric condition, involving 12 J/cm^2 E_d, 97% pulses' overlaps along the beam scanning and transverse directions, and 10 scanning passes, together with a thermally insulating baseplate, is capable of providing sub-micron level average surface roughness on selective laser melted aluminium alloy parts. This could be achieved within a reasonable processing time (~20 mins to polish a 10 × 10 mm^2 surface area). The duration is indeed much shorter than that would be required by conventional mechanical polishing methods for an equivalent reduction in SLM parts' surface roughness [30].

Following the surface roughness/quality assessments of the laser polished SLM ALSi10Mg parts the research further analyses the extended surface integrity aspects of the LP specimens, including residual stress, microhardness and microstructure. The residual stress analysis reveals that a reduction in the thermal gradient within the body during the cooling period after LP can shift the state of the residual stresses towards more neutral/compressive side with

respect to the tensile stresses of the as-built SLM parts which is often detrimental to the components' functional performance (e.g. fatigue failure [4]). Such decrease in the thermal gradient can be promoted either by increasing the heat input or by minimising the conductive heat dissipation from the body. However, undertaking the former route by increasing the laser energy density or the number of scanning passes beyond certain limits would deteriorate the surface quality. Conversely, the use of the ceramic plate clearly restricts the conductive heat dissipation (and thereby aids in maintaining a lower thermal gradient within the object) during the cooling period which leads to neutral/compressive stresses (−6.6 to −18.6 MPa) for the samples processed in air.

As surface oxidation is a typical phenomenon when laser polishing in atmospheric condition, this study further investigates the effects of using an inert gas environment during LP on the polished parts' surface integrity. The use of argon environment however does not provide any better surface quality compared to that achieved under the atmospheric condition, even with the presence of the ceramic plate under the samples. The flowing argon gas over the parts during LP evidently reduces the surface/sub-surface temperatures (~24% lower than that measured during LP in air), leading to inferior re-melting of material. The convective heat transfer from the parts under argon environment also increases the thermal gradient within the body during the cooling period after LP. Thus, the measured residual stresses within the specimens are tensile in nature (+3.1 to +27.1 MPa), although this is still lower than that of the parent SLM parts (+31.1 to +54.6 MPa).

As for the microhardness, laser polishing causes reduction in the sub-surface microhardness of the aluminium parts with respect to their bulk hardnesses, due to thermal softening. The thickness of the softened layer increased (up to a depth of ~35 μm from the top polished surface depending on the LP conditions) with an increase in the surface/sub surface temperatures, either because of the rise in the number of laser scans or when using the ceramic baseplate.

Microstructure assessments divulge the formation of white layers at the regions of lower sub-surface hardnesses (up to ~30 µm and ~22 µm when LP in air and argon, respectively, with the presence of the insulating plate). This is attributed to the re-distribution of Si-rich phases near the laser treated surface, leaving softer Al-rich phases within the white layer zones as revealed by the EDS and XPS analysis. Furthermore, the increase in the parts' bulk body temperatures due to the presence of the thermally insulating baseplate also causes reduction in the bulk hardenesses by ~15-25% compared to that of the SLM builds. This observation notably differs from the microhardness and microstructure analyses of the laser polished 3D printed SS316L and Ti-6Al-4V parts in the authors' previous study [31,32]. Sub-surface microhardnesses were higher than the bulk hardnesses for the LP steel samples while the polished Ti specimens exhibited substantial surface oxidation, together with numerous surface cracks when processed at an E_d of 9 J/cm^2. In contrast, minimal surface oxidation and cracks are observed on the LP aluminium samples processed with 12 J/cm^2 E_d and 10 scanning passes.

5. Conclusions

Research on the laser polishing of materials with high thermal conductivity, such as aluminium alloys, is extremely limited. The present study investigates nanosecond pulsed laser polishing of selective laser melted AlSi10Mg alloy parts. This aluminium alloy is chosen for its relevance to the production of lightweight aerospace, automotive and electronic components. In order to alleviate the challenges of laser polishing Al alloys, due to the materials' high thermal conductivity, diffusivity and reflectivity, this research proposes a novel strategy to improve the material's re-melting behaviour by employing a thermally insulating alumina ceramic baseplate under the specimens. The strategy aids in achieving sub-micron surface roughnesses (minimum S_a recorded 0.64 µm) of the parts that are ~80-88% lower than that of the SLM builds. The processing conditions associated with

these roughness values involve a 12 J/cm^2 laser energy density, 97% pulses' overlaps along the beam scanning as well as in transverse feed directions, and 10 scanning passes under atmospheric environment. The resulting surfaces exhibit fine laser scan track without any apparent signs of pits or cracks. It should also be noted that the extent of percentage reduction in roughness values depends on the initial roughness of the as-built SLM parts.

The proposed strategy of using a thermally insulating plate to improve material's re-melting implies that it is important to minimise conductive heat dissipation from the body in order to achieve greater effectiveness of laser polishing for highly thermally conductive materials. The proposed method is a proof-of-concept involving a simple scenario for rectangular/cubic objects with planner surfaces. The method can be adopted for LP of more complex, intricate AM parts by creating a pre-heated enclosed environment that would control the conductive and convective heat dissipation from the objects and would maintain the desired thermal gradient during the cooling period after polishing.

This study also brings the opportunity of measuring the surface temperature in real time (for example by using infrared temperature sensors) and controlling the material's responses during laser polishing. This could lead to several benefits for the parts' functional requirements, such as better tribological properties, improved corrosion resistance and fatigue life as consequences of the smoother surface topography and compressive residual stresses.

Acknowledgements

The research is supported by the European Union's Horizon 2020 Research and Innovation Programme under the grant agreement no. 723826 (MAESTRO) and Indian Institute of Technology Kharagpur's Shri Gopal Rajgarhia International Programme (SGRIP).

References

[1] U.M. Dilberoglu, B. Gharehpapagh, U. Yaman, M. Dolen, The role of additive manufacturing in the era of Industry 4.0, Procedia Manuf. 11 (2017) 545-554.

[2] U. Tradowsky, J. White, R.M. Ward, N. Read, W. Reimers, M.M. Attallah, Selective laser melting of AlSi10Mg: Influence of post-processing on the microstructural and tensile properties development, Mater. Des. 105 (2016) 212-222.

[3] A.H. Maamoun, Y.F. Xue, M.A. Elbestawi, S.C. Veldhuis, Effect of selective laser melting process parameters on the quality of Al alloy parts: Powder characterization, density, surface roughness, and dimensional accuracy, Materials 11 (2018) 2343.

[4] N.T. Aboulkhair, I. Maskery, C. Tuck, I. Ashcroft, N.M. Everitt, Improving the fatigue behaviour of a selectively laser melted aluminium alloy: Influence of heat treatment and surface quality, Mater. Des. 104 (2016) 174-182.

[5] C. Gu, Z. Jin, Y. Wang, R. Zhuang, X. Lu, S. Zhao, G. Zou, Polishing technology of surface for diamond film using the method of laser ablation, Chin. Sci. Bull. 42(23) (1997) 2010-2013.

[6] S.M. Pimenov, V.V. Kononenko, V.G. Ralchenko, V.I. Konov, S. Gloor, W. Lüthy, H.P. Weber, A.V. Khomich, Laser polishing of diamond plates, Appl. Phys. A 69 (1999) 81-88.

[7] O.Y. Bol'shepaev, N.N. Katomin, Laser polishing of glass articles, Glass Ceram. 54 (5-6) (1997) 141-142.

[8] W. Guo, M. Hua, P. Wai-Tat Tse, A.C.K. Mok, Process parameters selection for laser polishing DF2 (AISI O1) by Nd:YAG pulsed laser using orthogonal design, Int. J. Adv. Manuf. Technol. 59 (2012) 1009-1023.

[9] F.E. Pfefferkorn, N.A. Duffie, J.D. Morrow, Q. Wang, Effect of beam diameter on pulsed laser polishing of S7 tool steel, CIRP Ann. Manuf. Technol. 63 (1) (2014) 237-240.

[10] R. Avilés, J. Albizuri, A. Lamikiz, E. Ukar, A. Avilés, Influence of laser polishing on the high cycle fatigue strength of medium carbon AISI 1045 steel, Int. J. Fatigue 33 (2011) 1477-1489.

[11] M. Vadali, C. Ma, N.A. Duffie, X. Li, F.E. Pfefferkorn, Pulsed laser micropolishing: Surface prediction model, J. Manuf. Proc. 14 (2012) 307-315.

[12] A.M.K. Hafiz, E.V. Bordatchev, R.O. Tutunea-Fatan, Experimental analysis of applicability of a picosecond laser for micro-polishing of micromilled Inconel718 superalloy, Int. J. Adv. Manuf. Technol. 70 (2014) 1963-1978.

[13] C. Ma, M. Vadali, N.A. Duffie, F.E. Pfefferkorn, X. Li, Melt pool flow and surface evolution during pulsed laser micro polishing of Ti6Al4V, J. Manuf. Sci. Eng. ASME Trans. 135 (2013) 061023-1-8.

[14] J.A. Remos-Grez, D.L. Bourell, Reducing surface roughness of metallic free form-fabricated parts using non-tactile finishing methods, Int. J. Mater. Prod. Technol. 21 (4) (2004) 297-316.

[15] A. Lamikiz, J.A. Sánchez, L.N. López de Lacalle, J.L. Arana, Laser polishing of parts built up by selective laser sintering, Int. J. Mach. Tools Manuf. 47 (2007) 2040-2050.

[16] M.A. Obeidi, E. McCarthy, B. O'Connell, I. Ul Ahad, D. Brabazon, Laser polishing of additive manufactured 316L stainless steel synthesized by selective laser melting, Materials 12(6) (2019) 991.

[17] B. Rosa, P. Mognol, J.Y. Hascoet, Laser polishing of additive laser manufacturing surfaces, J. Laser Appl. 27 (2015) S29102.

[18] S. Marimuthu, A. Triantaphyllou, M. Antar, D. Wimpenny, H. Morton, M. Beard, Laser polishing of selective laser melted components, Int. J. Mach. Tools Manuf. 95 (2015) 97-104.

[19] C.P. Ma, Y.C. Guan, W. Zhou, Laser polishing of additive manufactured Ti alloys, Opt. Lasers Eng. 93 (2017) 171-177.

[20] C. Liang, Y. Hu, N. Liu, X. Zou, H. Wang, X. Zhang, Y. Fu, J. Hu, Laser polishing of Ti6Al4V fabricated by selective laser melting, Metals 10 (2020) 191.

[21] F. Zhihao, L. Libin, C. Longfei, G. Yingchun, Laser polishing of additive manufactured superalloy, Procedia CIRP 71 (2018) 150-154.

[22] M. Bures, M. Zetek, Application of laser surface polishing on additive manufactured parts of Inconel 718 nickel-based superalloy, MM Sci. J. March (2020) 3873-3877.

[23] B. Burzic, M. Hofele, S. Mürdter, H. Riegel, Laser polishing of ground aluminum surfaces with high energy continuous wave laser, J. Laser Appl. 29 (2017) 011701.

[24] S. Chen, B. Richter, J.D. Morrow, K. Sridharan, F.E. Pfefferkorn, M. Eriten, Pulsed laser remelting of A384 aluminum, part I: Measuring homogeneity and wear resistance, J. Manuf. Proc. 32 (2018) 606-614.

[25] M. Hofele, J. Schanz, B. Burzic, S. Lutz, M. Merkel, H. Riegel, Laser based post processing of additive manufactured metal parts, Lasers in Manuf. LIM 2017 Conference, Munich, Germany.

[26] J. Schmidt, R. Scholz, H. Riegel, Laser polishing of aluminum by remelting with high energy pulses, Mat.-wiss. u. Werkstofftech. 46(7) (2015) 686-691.

[27] M.A. Elahi, M. Koch, P. Plapper, Laser polishing of Aluminum and Polyamide for dissimilar laser welded assemblies, Lasers in Manuf. LIM 2019 Conference, Munich, Germany.

[28] G. Luo, H. Xiao, S. Li, C. Wang, Q. Zhu, L. Song, Quasi-continuous-wave laser surface melting of aluminium alloy: Precipitate morphology, solute segregation and corrosion resistance, Corrosion Sci. 152 (2019) 109-119.

[29] N. Read, W. Wang, K. Essa, M.M. Attallah, Selective laser melting of AlSi10Mg alloy: Process optimisation and mechanical properties development, Mater. Des. 65 (2015) 417-424.

[30] D. Bhaduri, P. Penchev, S. Dimov, K. Essa, L.N. Carter, C.I. Pruncu, J. Jiang, D. Pullini, On the surface integrity of additive manufactured and post-processed AlSi10Mg parts, Procedia CIRP 87 (2020) 339-344.

[31] D. Bhaduri, P. Penchev, A. Batal, S. Dimov, S.L. Soo, S. Sten, U. Harrysson, Z. Zhang, H. Dong, Laser polishing of 3D printed mesoscale components, Appl. Surf. Sci. 405 (2017) 29-46.

[32] D. Bhaduri, P. Penchev, S. Dimov, U. Harrysson, Laser polishing of 3D printed miniaturised titanium components, Proceedings of the 4M/IWMF Conference (2016), Lyngby, Denmark, 109-112.

[33] Materials Property Data. www.matweb.com. (Accessed on 10 January 2020).

[34] E. Yasa, J.-P. Kruth, J. Deckers, Manufacturing by combining selective laser melting and selective laser erosion/laser re-melting, CIRP Ann. Manuf. Technol. 60 (2011) 263-266.

[35] K.G. Prashanth, S. Scudino, H.J. Klauss, K.B. Surreddi, L. Löber, Z. Wang, A.K. Chaubey, U. Kühn, J. Eckert, Microstructure and mechanical properties of Al-12Si produced by selective laser melting: Effect of heat treatment, Mater. Sci. Eng. A 590 (2014) 153-160.

[36] D. Bhaduri, P. Penchev, S. Dimov, U. Harrysson, Pulsed laser polishing of 3D printed mesoscale parts, *presented at the 39th MATADOR Conference 2017, Manchester, UK*.